creased extreme events, but providing a means to link their occurrence with climate models.

REFERENCES AND NOTES

1. M. Parry and T. Carter, *Clim. Change* 7, 95 (1985); D. Cayan, J. Gardner, J. Landwehr, J. Namias, D. Peterson, in *Aspects of Climate Variability in the Pacific and the Western Americas*, D. Peterson, Ed. (Geophys. Monogr. 55, American Geophysical Union, Washington, DC, 1989), pp. xiii–xvi.
2. J. Hansen *et al.*, in *Coping with Climate Change*, J. Topping, Ed. (Climate Institute, Washington, DC, 1989), pp. 68–81; H. B. Gordon, P. H. Whetton, A. B. Pittock, A. M. Fowler, M. R. Haylock, *Clim. Dyn.* **8**, 83 (1992).
3. J. Knox, *Nature* **361**, 430 (1993).
4. V. Klemeš, in *Hydrology of Disasters*, O. Starosolszky and O. Melder, Eds. (James and James, London, 1989), pp. 43–51; V. R. Baker, *Nature* **361**, 402 (1993).
5. L. L. Ely, thesis, University of Arizona (1992).
6. ——— and V. R. Baker, *Phys. Geogr.* **6**, 103 (1985); J. E. O'Connor, J. E. Fuller, V. R. Baker, "Late Holocene flooding within the Salt River basin, central Arizona" (unpublished report to the Salt River Project, Tempe, AZ, 1986); J. E. O'Connor, R. H. Webb, V. R. Baker, *Geol. Soc. Am. Bull.* **97**, 410 (1986); J. B. Partridge and V. R. Baker, *Earth Surf. Processes Landforms* **12**, 109 (1987); L. K. Roberts, thesis, University of Arizona (1987); R. H. Webb, J. E. O'Connor, V. R. Baker, in *Flood Geomorphology*, V. R. Baker, R. C. Kochel, P. C. Patton, Eds. (Wiley, New York, 1988), pp. 403–418; E. E. Wohl, "Large floods in Redfield Canyon," contract IGA-89-6125-210-0111, Arizona Department of Water Resources (unpublished); T. S. Melis, thesis, Northern Arizona University (1990); Y. Enzel, L. L. Ely, J. Martinez-Goytre, R. G. Vivian, *J. Hydrol.*, in press.
7. V. R. Baker, *J. Hydrol.* **96**, 79 (1987).
8. There are notable differences between the flood record preserved in slackwater flood deposits and a conventional gaged discharge record. The latter records all flows but is limited in its depiction of the largest phenomena by the length of record and calibration problems with extremely high discharges. Slackwater deposits and paleostage indicators record only the largest events but over long time scales.
9. L. L. Ely, R. H. Webb, Y. Enzel, *Quat. Res.* **38**, 196 (1992).
10. Conventional ^{14}C dates are calculated assuming a constant atmospheric ^{14}C content, but fluctuations in atmospheric ^{14}C over the 5000-year period of this study have caused differences of up to 800 years between calculated ^{14}C ages and actual calendar-year dates. The ^{14}C dates in this study were converted to calendar years (in parentheses) with a calibration based on ^{14}C dates on tree rings of known ages [M. Stuiver and P. Reimer, *Radiocarbon* **28**, 1022 (1986)].
11. An increase in floods in the last 100 years is consistent with other paleohydrological evidence from the Southwest in which the early 1900s stands out as a period of exceptionally high annual runoff in dendrohydrological records covering 500 to 2000 years [R. D. D'Arrigo and G. C. Jacoby, *Holocene* 1, 95 (1991)], as well as a period of regional channel incision [R. Cooke and R. Reeves, *Arroyos and Environmental Change in the American Southwest* (Clarendon, Oxford, United Kingdom, 1976); R. H. Webb, S. S. Smith, V. A. S. McCord, *Grand Canyon Nat. Hist. Assoc. Monogr. 9* (1991)].
12. F. Röthlisberger, *10,000 Jahre Gletschergeschichte der Erde* (Verlag Sauerlander, Aarau, Switzerland, 1986); T. Wigley, in *Secular Solar and Geomagnetic Variations in the Last 10,000 Years*, F. Stephenson and A. Wolfendale, Eds. (Kluwer, Dordrecht, Netherlands, 1988), pp. 209–224.
13. T. R. Van Devender, R. S. Thompson, J. L. Betancourt, in *North America and Adjacent Oceans During the Last Deglaciation*, W. Ruddiman and H. Wright Jr., Eds. (Geological Society of America, Boulder, CO, 1987), pp. 323–352; P. T. Davis, *Quat. Sci. Rev.* 7, 129 (1988).
14. J. M. Grove, *The Little Ice Age* (Methuen, New York, 1988).
15. P. J. Mehringer Jr. and C. N. Warren, in "Holocene environmental change in the Great Basin," *Nev. Archeol. Surv. Res. Pap. No. 6*, R. Elston and P. Headrick, Eds. (1976), pp. 121–150; G. Smith, *U.S. Geol. Surv. Prof. Pap. 1043* (1979); L. Benson and H. Klieforth, in *Aspects of Climate Variability in the Pacific and the Western Americas*, D. H. Peterson, Ed. (Geophys. Monogr. 55, American Geophysical Union, Washington, DC, 1989), pp. 41–59; M. R. Waters, *Quat. Res.* **32**, 1 (1989); S. Stine, *Palaeogeogr. Palaeoclim. Palaeoecol.* **78**, 333 (1990).
16. Y. Enzel, D. R. Cayan, R. Y. Anderson, S. G. Wells, *Nature* **341**, 44 (1989).
17. The Holocene lakes in Silver Lake playa (Fig. 2) are directly related to an increased frequency of large winter floods on the Mojave River [(*16*); Y. Enzel, *Holocene* **2**, 11 (1992)], which occur under atmospheric circulation patterns also conducive to floods in Arizona (*22*) (Fig. 3A).
18. K. K. Hirschboeck, thesis, University of Arizona (1985).
19. R. H. Webb and J. L. Betancourt, *U.S. Geol. Surv. Water-Supply Pap. 2379* (1992).
20. J. E. Kutzbach and P. J. Guetter, *J. Atmos. Sci.* 43, 1726 (1986).
21. D. R. Cayan and R. H. Webb, in *El Niño: Historical and Paleoclimatic Aspects of the Southern Oscillation*, H. Diaz and V. Markgraf, Eds. (Cambridge Univ. Press, Cambridge, 1993), pp. 29–68.
22. L. L. Ely, Y. Enzel, D. R. Cayan, *J. Clim.*, in press.
23. R. Y. Anderson, in *El Niño: Historical and Paleoclimatic Aspects of the Southern Oscillation*, H. Diaz and V. Markgraf, Eds. (Cambridge Univ. Press, Cambridge, 1993), pp. 193–200; W. H. Quinn, *ibid.*, pp. 119–149.
24. N. Pisias, *Quat. Res.* **10**, 366 (1978).

25. Research supported by the National Science Foundation Engineering Directorate, Natural and Manmade Hazards Mitigation Program (grant BCS-8901430) (V.R.B.), Geological Society of America (L.L.E.), and Sigma Xi Scientific Research Society (L.L.E.). We thank J. O'Connor and R. Webb for assistance and discussion and E. Bainto for circulation computations. Contribution no. 21 of the Arizona Laboratory for Paleohydrological and Hydroclimatological Analysis (ALPHA).

24 May 1993; accepted 4 August 1993

Latest Pleistocene and Holocene Geomagnetic Paleointensity on Hawaii

Edward A. Mankinen and Duane E. Champion

Geomagnetic paleointensity determinations from radiocarbon-dated lava flows on the island of Hawaii provide an estimate of broad trends in paleointensity for Holocene time and offer a glimpse of intensity variations near the end of the last glacial period. When the data from Hawaii are compared with others worldwide, the intensity of the geomagnetic field seems to have been reduced from the Holocene average by about 35 percent between 45,000 and 10,000 years ago. A long-term reduction of this magnitude is compatible with reported increases in the production rate of cosmogenic nuclides during the same interval.

Because radiocarbon (^{14}C) is one of several nuclides produced in the upper atmosphere by cosmic radiation, its abundance can be affected in a number of ways (*1*). To correct for these variations, researchers have well calibrated ^{14}C ages to about 9000 years before present (B.P.) and tentatively to about 13,000 years B.P., by comparison with tree-ring and glacial-varve chronologies (*2*). In an attempt to calibrate the ^{14}C time scale to older periods, a comparison was made of ages determined by the ^{14}C (*3*) and ^{234}U-^{230}Th (*4*) techniques on a sequence of cores from coral reefs off the island of Barbados. The ages were in general agreement for the last 9000 years, but the U-Th ages were consistently older than the ^{14}C ages in older material, with a maximum discrepancy of 3500 years at 20,000 years B.P. If the U-Th ages are correct, the concentration of ^{14}C in the atmosphere must have been about 40% larger than it is now. A study of sedimentary cores from the Pacific Ocean indicates that the global production of ^{10}Be was at least 25% greater during this same interval (*5*). The only factor that seems to function in producing such large increases in the amount of cosmogenic nuclides is a substantial decrease in the intensity of the geomagnetic field, which would allow an increased flux of cosmic rays to impinge on the Earth's upper atmosphere (*1, 4, 5*).

Little is known about variations in geomagnetic intensity over much of geologic time because of the difficulties in obtaining dated material that retains an accurate intensity record and because of the time-consuming nature of the experimental procedures. Absolute values of paleointensity can be obtained only from rocks and archaeological artifacts that have acquired a thermoremanent magnetization (TRM) upon cooling in the Earth's magnetic field. The paleointensity record from many globally distributed locations must be averaged to eliminate the effects of nondipole variations so that a true picture of the global (dipole) field can be obtained.

U.S. Geological Survey, Mail Stop 937, 345 Middlefield Road, Menlo Park, CA 94025.

Fig. 1. Typical examples of paleointensity data (NRM-TRM diagrams) from (**A**) the lower temperature phase of samples containing two titanomagnetite populations (specimen 6B012-2) and (**B**) samples that have undergone high-temperature deuteric oxidation (specimen 9B990-1). Circles are NRM-TRM points calculated for each double heating at the temperature (in Celsius) indicated near each point. The NRM in these diagrams is the component of remanence directed along the stable NRM direction, and the TRM is the component projected onto the applied field direction. Lines connect each PTRM check (triangles) to the NRM-TRM point that corresponds to the maximum temperature to which the sample was heated before the check was performed. Solid circles are points used to determine the least squares line (shown as the heavy, solid line); open circles are points not used in the calculations.

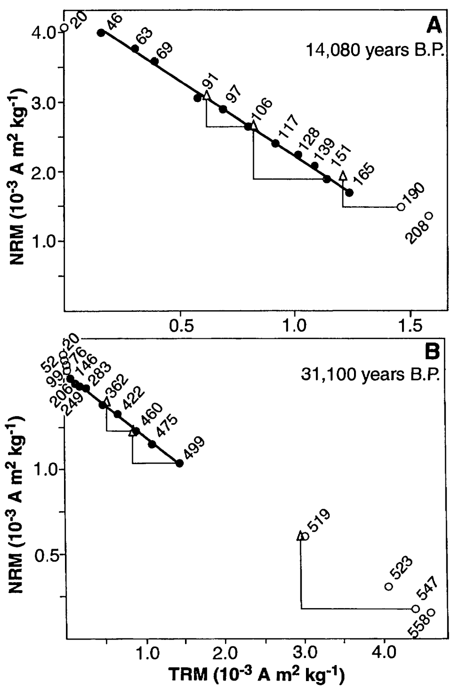

Many paleointensity data are available for the last several thousand years because of detailed geomagnetic secular variation studies at numerous archaeological sites; data from pre-Holocene time, however, are scarce. Analysis of the archaeomagnetic data (6) led to a description of dipole variations for Holocene time (*7*). Because every absolute paleointensity measurement represents an instantaneous reading of the geomagnetic field and the determinations are unevenly distributed over time, attempts have been made to obtain continuous intensity records from sedimentary sequences. At best, such records provide relative, and often very approximate, paleointensities because the natural processes by which sediment becomes magnetized are poorly understood. However, when the samples are carefully selected (8, 9) relative paleointensity records show broad similarities to the worldwide archaeomagnetic record (*10–13*) and indicate that intensities were very low at times between 140,000 and 10,000 years ago (140 to 10 ka). Using the relative paleointensity record from the Eastern Mediterranean (*12*) to model the content of ^{14}C in the atmosphere, Mazaud *et al.* (*14*) found that ^{14}C ages between 40 and 18 ka could be too young by about 2 to 3 ka, which qualitatively supports the conclusions based on the isotopic record.

To investigate geomagnetic paleointensity variations immediately preceding Holocene time and to help evaluate the validity of the sedimentary record, we performed experiments on six ^{14}C-dated lava flows on Hawaii that range in age from 31,100 to 13,530 years B.P. Although strong nondipole fields were present in the vicinity of Hawaii from about 5000 to 200 years ago (*15–17*), they seem to have been absent between about 12,000 and 5000 years B.P. (*17*) just as they have been during the past approximately 160 years (*18, 19*). Because the nondipole field seems to have been weak or absent in the vicinity of Hawaii over substantial periods of time, the possibility exists that paleointensity studies there could provide a first approximation of dipole field strength for intervals where few data are available.

Absolute measurements of intensity require the original thermoremanence to be compared with a remanence that is artificially acquired in a known field. We used the method developed by Thellier and Thellier (*20*) as modified by Coe (*21, 22*). Typical examples of our paleointensity data are dis-

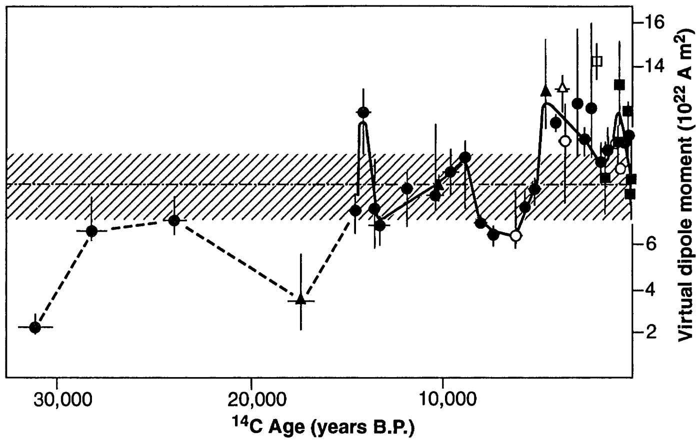

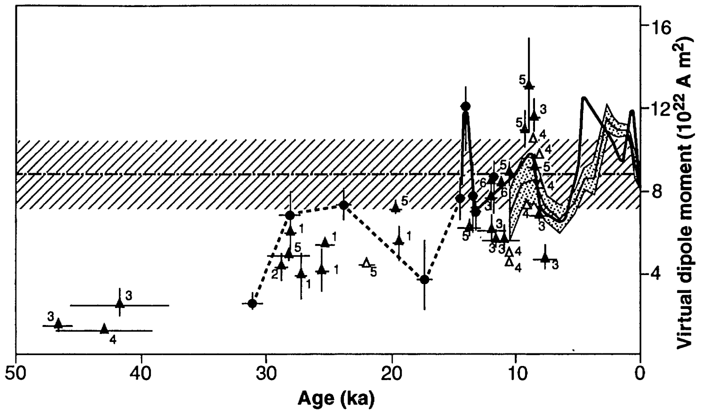

Fig. 2 (left). VDMs as a function of age for the Hawaiian ^{14}C-dated lava flows. Ages were calculated with the 5568-year half-life for ^{14}C and have not been corrected for isotopic fractionation or secular changes in atmospheric ^{14}C. Circles are weighted means from Table 1 and (*17*); triangles are data from (*15*); squares are data from (*16*). Open symbols are values based on fewer than three determinations; the curve is a rough fit (by eye) to all data and is dashed where the data are not well constrained; the dashed horizontal line is the worldwide average VDM for the past 10,000 years (*6*) and its standard deviation (ruled area). **Fig. 3 (right).** Hawaiian VDM curve from Fig. 2 compared with available data worldwide up to 50 ka. The dotted pattern is the 95% confidence envelope about the worldwide mean curve for Holocene time (*6*) based on the archaeomagnetic record. The large circles are data from Hawaiian lava flows that are older than 11 ka; the small triangles are data from other localities as noted. Open symbols denote less reliable data. Data points of flows with ages between 10 and 8 ka are those published since the compilation of McElhinny and Senanayake (*6*) and are not included in the worldwide average. 1, Data from Australia (*32, 34*); 2, from Czechoslovakia (*42*); 3, from France (*33, 36, 44, 46*); 4, from Iceland (*30, 38, 41*); 5, from Japan (*31, 45, 48*); and 6, from the western United States (*29*).

played on natural remanent magnetization (NRM)–TRM diagrams (23) shown in Fig. 1. For an ideal sample, all NRM-TRM points will fall on a straight line with the negative slope equal to the ratio of the intensity of ancient Earth's field to that of the applied laboratory field. In practice, however, magnetochemical changes routinely occur during the laboratory heatings and only a fraction of the total NRM can be used to estimate the paleointensity (24). The reliability of our results was assessed by (i) the linearity of the NRM-TRM diagram, (ii) the consistency of partial-TRM (PTRM) checks (20), (iii) the amount of chemical remanent magnetization (CRM) acquired (25), (iv) changes in low-field magnetic susceptibility, (v) within-flow consistency, and (vi) analytical precision (15). Only 3 of the 30 samples analyzed failed to yield an estimate of the paleofield (26).

We calculated a virtual dipole moment (VDM) (27) using each weighted data point of mean paleointensity given in Table 1 (28). These points are shown in Fig. 2 as are the data from other studies on Hawaii (15–17). Of the nine pre-Holocene flows, only the lava from 14,080 years B.P. (Table 1) yields a paleointensity that is clearly above the worldwide average VDM for the past 10,000 years (6). Six of the flows record low normal paleointensities, whereas those flows that erupted 31,100 (Table 1) and 17,360 (15) years B.P. indicate cooling in anomalously low paleofields. Although paleointensity data could not be calculated for two of the five samples from the 14,080-year-B.P. flow, the remaining samples provided seemingly reliable results (Fig. 1A). Because there is no apparent reason to suspect the results from this flow, we believe that its higher value represents a brief pulse that reflects the nondipole field similar to that at about 700 years ago (Fig. 2).

To assess the intensity variations during latest Pleistocene to Holocene times, we compared (Fig. 3) the Hawaiian curve (Fig. 2) to a worldwide dipole variation curve for Holocene time (6) and all available data for 50 to 11 ka. We excluded the oldest point on the dipole variation curve because it was based on only two data points (from the western United States) (29). We included data from between 10,000 and 8000 years ago that were published after publication of the previous compilation (6). Ages shown were determined by the ^{14}C, thermoluminescence, tephrochronology, K-Ar, or $^{40}Ar/^{39}Ar$ methods. Because curves calibrated with ^{14}C are not well defined for ages greater than 9000 years B.P., the ^{14}C ages shown in Fig. 3 are uncorrected and, therefore, not directly comparable to ages determined by the other methods. The ^{14}C ages older than 10,000 years will probably need to be revised to older ages. Less reliable data points in the 10,000- to 8000-year interval are those for the Icelandic lava flows (30), for which few details of dating or paleointensity determinations were provided; similarly, the value for the 22,000-year-old pyroclastic flow from Japan (31) was based on two specimens from a single, unoriented hand sample. We also excluded the data from four aboriginal fireplaces in southeastern Australia that record the Lake Mungo

Table 1. Paleointensity data from ^{14}C-dated lava flows on Hawaii. The ^{14}C ages are from (49); N is the number of points in the $T_{mn} - T_{mx}$ interval, where T_{mn} and T_{mx} are the minimum and maximum, respectively, of the temperature range used to determine paleointensity; f, g, and q are NRM fraction, gap factor, and quality factor, respectively (15); F_e is the paleointensity estimate for an individual specimen, and $\sigma(F_e)$ is its standard deviation (20); $\bar{F}_e$ is the unweighted average paleointensity ± SD; $\langle F_e \rangle$ is the weighted average paleointensity derived with the use of the weighting factor of (47); VDM is the virtual dipole moment (27).

^{14}C age (years B.P.)	^{14}C number	Sample number	N	T_{mn} (°C)	T_{mx} (°C)	f	g	q	$F_e \pm \sigma(F_e)$ (μT)	$\bar{F}_e$ ± SD (μT)	$\langle F_e \rangle$ (μT)	VDM (10^{22} A m^2)
13,530 ± 180	W4627	6B013-3	7	351	521	0.427	0.823	8.7	43.9 ± 1.8			
		6B015-3	9	26	118	0.618	0.837	19.2	26.7 ± 0.7			
		6B016-2	10	29	145	0.436	0.871	7.9	27.6 ± 1.3	30.9 ± 7.6	30.9	7.70
		6B017-3	11	44	163	0.423	0.833	6.9	31.2 ± 1.6			
		6B018-3	8	44	127	0.389	0.782	4.7	25.1 ± 1.6			
14,080 ± 150	W4971	6B001-2				No good						
		6B003-2				No good						
		6B006-2	11	47	170	0.605	0.877	16.3	43.9 ± 1.4	47.0 ± 6.3	49.3	11.99
		6B010-4	10	47	154	0.400	0.864	5.0	42.8 ± 2.9			
		6B012-2	11	45	165	0.529	0.885	24.7	54.2 ± 1.0			
14,500 ± 200	W4620	6B026-3	7	30	90	0.514	0.800	5.8	25.0 ± 1.8			
		6B027-3	11	44	175	0.614	0.891	36.0	32.4 ± 0.5			
		6B029-3	13	26	178	0.605	0.894	25.4	31.3 ± 0.7	29.8 ± 3.3	31.1	7.59
		6B030-3	9	45	123	0.308	0.836	5.8	30.4 ± 1.4			
		6B036-4				No good						
23,840 ± 600	W4360	6B049-2	13	26	180	0.694	0.898	26.5	25.7 ± 0.6			
		6B051-2	8	29	91	0.529	0.787	6.5	26.1 ± 1.7			
		6B052-3	11	30	145	0.793	0.860	18.7	30.0 ± 1.1	29.2 ± 3.6	28.3	7.19
		6B055-2	10	30	125	0.341	0.851	3.5	29.8 ± 2.5			
		6B056-2	10	29	124	0.437	0.870	6.0	34.6 ± 2.2			
28,150 ± 800	W4368	9B997-1	14	42	221	0.603	0.901	24.3	27.5 ± 0.6			
		9B999-1	11	45	164	0.583	0.880	38.4	26.2 ± 0.3			
		9A000-1	10	44	144	0.322	0.875	3.2	35.1 ± 3.1	28.9 ± 3.7	27.2	6.67
		9A007-3	14	43	221	0.732	0.915	39.5	29.5 ± 0.5			
		9A008-3	16	44	262	0.774	0.922	89.4	26.1 ± 0.2			
31,100 ± 900	W3935	9B985-1	14	84	292	0.651	0.909	26.2	8.3 ± 0.2			
		9B990-1	9	146	498	0.321	0.835	16.3	9.3 ± 0.2			
		9B991-1	10	149	518	0.356	0.824	8.0	9.6 ± 0.4	9.9 ± 1.7	9.5	2.39
		9B992-1	10	100	500	0.263	0.855	7.7	12.8 ± 0.4			
		9B994-1	8	100	455	0.402	0.734	9.2	9.6 ± 0.3			

excursion (*32*) at about 30,000 years B.P. These fireplaces yield paleointensities that are three times the strength of the present Earth's field and are, therefore, unlikely to be representative of the geomagnetic dipole. It also has been suggested (*33*) that anomalous paleomagnetic results from Lake Mungo may be the result of lightning strikes. We excluded a low paleointensity (*34*) determined for sediment baked by the Coulée de Boissejour (France), because the age of the flow is poorly constrained (*35*).

Some of the lowest paleointensities during this period have been obtained from the reversed-polarity Laschamp and Olby (*33*) and the intermediate-polarity Louchadière (*36*) lava flows in the Chaîne des Puys (France). These lava flows erupted during the Laschamp geomagnetic excursion (*37*), with an age (determined by the K-Ar and $^{40}Ar/^{39}Ar$ methods) of 46.6 ± 1.2 ka (*38*). A low paleointensity (not shown in Fig. 3) was also obtained from sediment baked by the Royat flow (*34*), which was correlated with the Laschamp and Olby flows because of anomalous magnetization directions and similar thermoluminescence ages (≅ 33 ka) (*35*). New age determinations for the Laschamp excursion (*38*) would seem to discount this possibility, but recent studies (*36, 39*) indicate that the Royat flow also may have erupted between 46 and 40 ka and indeed may be correlative. Basalt flows recording the Skalamaelifell excursion (*40*) on the Reykjanes Peninsula (Iceland) have low paleointensities (*38, 41*), a weighted mean age (K-Ar method) of 42.9 ± 3.9 ka (*33*), and thus probably are equivalent to the Chaîne des Puys flows. The intensity indicated by these studies is about 20% of the Holocene average. Although low paleointensities are expected during excursions of the geomagnetic field, the low value for the 31,100-year-B.P. basalt from Hawaii (Table 1 and Fig. 3) suggests that the extreme low recorded by the Laschamp excursion flows may have lasted significantly longer than the estimated several-hundred-year duration (*38, 39*) of the geomagnetic excursion. A relative paleointensity record in sedimentary cores from Lac du Bouchet (*39*) in the Massif Central, France, also indicates a long period of low intensity between 43 and 30 ka. There is a critical need for additional data from 40 to 30 ka to determine if these conclusions are valid.

After this period of very low paleointensities, the geomagnetic field was stronger from about 29 to 19 ka (Fig. 3). Included within this age range are 11 data points from baked earth in Czechoslovakia (*42*), aboriginal fireplaces in Australia (*32, 43*), pyroclastic flows in Japan (*31*), and lava flows in Hawaii (Table 1). These sites were all dated with the ^{14}C method. The intensity of the geomagnetic field was about 60% of normal during this interval. The field may have weakened again, as evidenced by the single Hawaiian lava flow dated at 17,360 years B.P., whose VDM (*15*) is approximately 40% of the Holocene average.

Twelve paleointensity determinations are available for the period between about 15 and 11 ka. These were obtained from hearths at Etiolles and Marsangy, France (*44*), and from lava flows of Fuji Volcano, Japan (*45*), Chaîne des Puys (*46*), the western United States (*29*), and Hawaii (Table 1) (*15*). The Chaîne des Puys lava flows were dated by thermoluminescence, the other lavas by ^{14}C, and the hearths by a combination of ^{14}C and archaeological methods. An average of these 12 VDMs is 85% of the average field and well within the range of normal secular variation. Field intensity then increased to a well-defined peak at about 9000 years B.P. (Fig. 3) (*45, 46*).

Paleointensity estimates on the 31.1 to 13.5 ka Hawaiian lava flows in general seem comparable to the few data that are available from other parts of the world. Similarities also are seen between these absolute paleointensities and the relative paleointensity record from some marine cores (*12, 13*) that show minima at about 39 and 18 ka in the age range shown in Fig. 3. Thus, both types of records lend considerable weight to earlier indications that geomagnetic intensity was anomalously weak for some thousands of years immediately before Holocene time.

Radiocarbon produced by the interaction of cosmic rays with nitrogen in the upper atmosphere is mixed continuously in the atmosphere, biosphere, and oceans. Its concentration in any of these carbon reservoirs is determined by the production rate, radioactive decay, and exchange rate between the reservoirs. Because the yearly production is only a small fraction of the total ^{14}C inventory, short-term perturbations in production have a minor influence in total atmospheric concentration, whereas long-term (10^3 years) variations are needed to cause the discrepancies between the dating methods as noted above. The data (Fig. 3) imply that the geomagnetic field was reduced, on average, by about 35% between 45 and 10 ka; this conclusion is compatible with reported increases in the production rate of cosmogenic nuclides during the same interval.

REFERENCES AND NOTES

1. M. Stuiver, T. F. Braziunas, B. Becker, B. Kromer, *Quat. Res.* **35**, 1 (1991).
2. M. Stuiver, B. Kromer, B. Becker, C. W. Ferguson, *Radiocarbon* **28**, 969 (1986).
3. R. G. Fairbanks, *Nature* **342**, 637 (1989).
4. E. Bard, B. Hamelin, R. G. Fairbanks, A. Zindler, *ibid.* **345**, 405 (1990).
5. Y. Lao *et al.*, *ibid.* **357**, 576 (1992).
6. M. W. McElhinny and W. E. Senanayake, *J. Geomagn. Geoelectr. Kyoto* **34**, 39 (1982).
7. Although some Holocene paleomagnetic data are available from different parts of the world, the dipole variation curve remains heavily biased toward the European region.
8. S. Levi and S. K. Banerjee, *Earth Planet. Sci. Lett.* **29**, 219 (1976).
9. J. W. King, S. K. Banerjee, J. Marvin, *J. Geophys. Res.* **88**, 5911 (1983).
10. C. G. Constable and L. Tauxe, *Geophys. J. R. Astron. Soc.* **90**, 43 (1987).
11. L. Tauxe and J.-P. Valet, *Phys. Earth Planet. Inter.* **56**, 59 (1989).
12. E. Tric *et al.*, *J. Geophys. Res.* **97**, 9337 (1992).
13. L. Meynadier, J.-P. Valet, R. Weeks, N. J. Shackleton, V. L. Hagee, *Earth Planet. Sci. Lett.* **114**, 39 (1992).
14. A. Mazaud, C. Laj, E. Bard, M. Arnold, E. Tric, *Geophys. Res. Lett.* **18**, 1885 (1991).
15. R. S. Coe, C. S. Grommé, E. A. Mankinen, *J. Geophys. Res.* **83**, 1740 (1978).
16. H. Tanaka and M. Kono, *J. Geomagn. Geoelectr. Kyoto* **43**, 375 (1991).
17. E. A. Mankinen and D. E. Champion, *J. Geophys. Res.* **98**, 7959 (1993).
18. T. Yukutake and H. Tachinaka, *Bull. Earthquake Res. Inst. Univ. Tokyo* **47**, 65 (1969).
19. R. R. Doell and A. Cox, in *The Nature of the Solid Earth*, E. C. Robertson, Ed. (McGraw-Hill, New York, 1972), chap. 11.
20. E. Thellier and O. Thellier, *Ann. Geophys.* **15**, 285 (1959).
21. R. S. Coe, *J. Geomagn. Geoelectr. Kyoto* **19**, 157 (1967).
22. Specimens were initially heated to a predetermined temperature and cooled in a low ambient field less than 100 nT. An external field of 25 μT was applied parallel to the cylindrical axes of the specimens during a second heating to the same temperature. Measurements were made at room temperature with a superconducting magnetometer, and the ratio of NRM lost to TRM gained was determined for each of the paired heatings. The experiments were performed in a nitrogen atmosphere to inhibit oxidation.
23. T. Nagata, Y. Arai, K. Momose, *J. Geophys. Res.* **68**, 5277 (1963).
24. Because a recently acquired viscous remanent magnetization (VRM) can be close to the TRM direction and difficult to detect, the initial room-temperature measurement was not included in any of the paleointensity estimates even if it fell on the same line as subsequent NRM-TRM points.
25. R. S. Coe, C. S. Grommé, E. A. Mankinen, *J. Geophys. Res.* **89**, 1059 (1984).
26. Geometric mean values (*17*) of the ratio of saturation remanence to saturation magnetization (0.18), of the Koenigsberger ratio (*45*), and of the median destructive field (30 mT) indicate that the Hawaiian basalts contain primarily single-domain particles that are ideal for paleointensity experiments. Linear segments on the NRM-TRM diagrams were defined by a minimum of seven points and spanned a range of 26 to 79% of the total NRM intensity. Potential effects from a CRM acquired during the heating experiments (*25*) would cause errors in the paleointensity estimates ranging from 0 to 16% (mean = 4%) in the linear segments analyzed. Changes in low-field magnetic susceptibility were less than 25%.
27. P. J. Smith, *Geophys. J. R. Astron. Soc.* **12**, 321 (1967).
28. Because the weighting factor used differs from the weight derived from the theory of errors, it cannot, therefore, be used to calculate a weighted standard error. We followed the method of Prévot *et al.* (*47*) and expressed the uncertainties of the VDMs in Fig. 2 as the standard deviation about the unweighted mean, calculated from individual paleointensity determinations.
29. D. E. Champion, *U.S. Geol. Surv. Open-File Rep. 80-824* (1980).
30. Ch. Schweitzer and H. C. Soffel, *J. Geophys.* **47** 57 (1980).
31. H. Tanaka, *Rock Magn. Paleogeophys.* **5**, 95 (1978).

32. M. Barbetti and M. McElhinny, *Philos. Trans. R. Soc. London Ser. A* **281**, 515 (1976).
33. P. Roperch, N. Bonhommet, S. Levi, *Earth Planet. Sci. Lett.* **88**, 209 (1988).
34. M. Barbetti and K. Flude, *Nature* **278**, 153 (1979).
35. J. Huxtable, M. J. Aitken, N. Bonhommet, *ibid.* **275**, 207 (1978).
36. A. Chauvin, R. A. Duncan, N. Bonhommet, S. Levi, *Geophys. Res. Lett.* **16**, 1189 (1989).
37. N. Bonhommet and J. Babkine, *C. R. Acad. Sci. Paris* **264**, 92 (1967).
38. S. Levi *et al.*, *Earth Planet. Sci. Lett.* **96**, 443 (1990).
39. N. Thouveny and K. M. Creer, *Geology* **20**, 399 (1992).
40. L. Kristjansson and A. Gudmundsson, *Geophys. Res. Lett.* **7**, 337 (1980).
41. M. Marshall, A. Chauvin, N. Bonhommet, *J. Geophys. Res.* **93**, 11681 (1988).
42. V. Bucha, *Archaeometry* **10**, 12 (1967).
43. M. Barbetti and K. Flude, *Nature* **279**, 202 (1979).
44. M. Barbetti, Y. Taborin, B. Schmider, K. Flude, *Archaeometry* **22**, 25 (1980).
45. H. Tanaka, *J. Geophys. Res.* **95**, 17517 (1990).
46. J.-S. Salis, N. Bonhommet, S. Levi, *ibid.* **94**, 15771 (1989).
47. M. Prévot, E. A. Mankinen, R. S. Coe, C. S. Grommé, *ibid.* **90**, 10417 (1985).
48. M. Kono, *J. Geomagn. Geoelectr. Kyoto* **23**, 1 (1971).
49. M. Rubin, L. Kelley-Gargulinski, J. P. McGeehin, *U.S. Geol. Surv. Prof. Pap. 1350* (1987).
50. We thank R. S. Bogar for assistance with the paleointensity experiments and R. S. Coe, C. S. Grommé, J. W. Hillhouse, S. Levi, and one anonymous referee for constructive reviews.

8 June 1993; accepted 18 August 1993

Structural Features of Polysaccharides That Induce Intra-Abdominal Abscesses

Arthur O. Tzianabos,* Andrew B. Onderdonk, Bernard Rosner, Ronald L. Cisneros, Dennis L. Kasper

The capsular polysaccharide complex from *Bacteroides fragilis* promotes the formation of intra-abdominal abscesses—a pathologic host response to infecting microorganisms. This complex consists of two distinct polysaccharides, each with repeating units that have positively charged amino groups and negatively charged carboxyl or phosphate groups. Analysis of these polysaccharides as well as other charged carbohydrates before and after chemical modification revealed that these oppositely charged groups are required for the induction of intra-abdominal abscesses in a rat model.

The mechanisms by which bacterial pathogens induce specific disease processes are often poorly understood. Intra-abdominal abscess formation caused by *Bacteroides fragilis* is an example of a pathologic host response to infection. In this tissue reaction, a fibrous capsule localizes invading bacteria and presumably protects the host from disseminated infection. These abscesses cause substantial morbidity and mortality, are difficult to treat with antimicrobial therapy, and usually require surgical intervention (*1*).

Although *B. fragilis* makes up less than 0.5% of the normal colonic microflora, it is the predominate obligate anaerobe isolated from human infections such as intra-abdominal sepsis and bacteremia (*2, 3*). In rodent models, intraperitoneal administration of *B. fragilis* or its capsular polysaccharide complex (CPC) promotes the formation of intra-abdominal abscesses (*4*). Abscesses formed in response to the CPC are bacteriologically sterile yet histologically identical to abscesses formed in response to intact bacteria. Although most bacterial polysaccharides are considered to be T cell–independent antigens that elicit humoral responses, the CPC promotes abscess formation and confers immunity to abscess induction in a T cell–dependent manner (*5*).

The CPC of *B. fragilis* 9343 exhibits unusual chemical and immunochemical characteristics (*6, 7*). Recently, we have shown that this complex consists of two distinct high molecular weight polysaccharides, termed A and B (*8*). Each is composed of multiple repeating units of oligosaccharides that have uncommon constituent sugars with free amino, carboxyl, and phosphate groups (*9*) (Fig. 1). Polysaccharide A has a tetrasaccharide repeating unit with a balanced positively charged amino group and negatively charged carboxyl group (Fig. 1A). Polysaccharide B has a hexasaccharide repeating unit, including an unusual 2-aminoethylphosphonate substituent containing a free amino group and a negatively charged phosphate group. The galacturonic acid residue contains an additional negatively charged carboxyl group (Fig. 1B). Ionic interactions between the two saccharide chains tightly link polysaccharides A and B into a high molecular weight complex (*10*). Further study has shown that all strains of *B. fragilis* examined thus far also have a complex of at least two different polysaccharides that are antigenically diverse while some strains show cross-reactivity with the 9343 CPC (*11*).

We hypothesized that the unusual structural features of the CPC are critical to abscess formation, and therefore tested polysaccharide A and B and the CPC for the ability to induce abscesses in a rat model of intra-abdominal sepsis (*12*). Rats were injected intraperitoneally with each polymer, and the dose required to induce abscesses in 50% of the animals (AD_{50}) was determined. In this assay, polysaccharide A was an order of magnitude more active (AD_{50} = 0.67 μg) than polysaccharide B (AD_{50} = 25 μg) or the CPC (AD_{50} = 22 μg) (Table 1).

Table 1. Abscess induction by *B. fragilis* polysaccharides. Rats were administered 10-fold dilutions of each polysaccharide mixed 1:1 with a sterile cecal contents adjuvant (*4, 12*) and examined 6 days later for the formation of intra-abdominal abscesses. Rats receiving saline (no polysaccharide) and adjuvant did not form abscesses in these experiments. Data were accumulated from two separate experiments. Experiment 1: *B. fragilis* component polysaccharides and the CPC were tested. The AD_{50} values were calculated by the method of Reed and Muench (*25*). Experiment 2: Chemically modified versions of polysaccharide A were tested in the rat model. Chemical modifications of polysaccharide A are detailed in Fig. 1A. The AD_{50} and *P* values were calculated with the use of a mathematical model based on logistic regression analysis (*26*). ND, not done.

Polysaccharide	Fraction of rats with abscesses at a dose of					AD_{50} (μg)	*P*
	200 μg	20 μg	2 μg	0.2 μg	0.02 μg		
			Experiment 1				
A (native)	31/38	18/25	21/38	7/18	2/19	0.67	—
B	23/29	14/30	5/28	ND	ND	25	—
CPC	23/28	10/19	6/20	ND	ND	22	—
			Experiment 2				
A (native)	16/20	14/20	10/19	ND	ND	1.3	—
A (reduced)	5/20	2/19	2/19	ND	ND	>200	<0.0005*
A (*N*-acetylated)	7/20	3/19	1/17	ND	ND	>200	<0.0005*
A (deaminated)	7/20	6/18	3/19	ND	ND	>200	<0.0005*

*As compared with polysaccharide A (native).

A. O. Tzianabos, B. Rosner, R. L. Cisneros, Channing Laboratory, Brigham and Women's Hospital, and Department of Medicine, Harvard Medical School, Boston, MA 02115.
A. B. Onderdonk, Channing Laboratory, Brigham and Women's Hospital, and Department of Pathology, Harvard Medical School, Boston, MA 02115.
D. L. Kasper, Channing Laboratory, Brigham and Women's Hospital, and Division of Infectious Diseases, Beth Israel Hospital, Harvard Medical School, Boston, MA 02115.

*To whom correspondence should be addressed.